Received: Added at production | Revised: Added at production | Accepted: Added at production
DOI: xxx/xxxx

RESEARCH ARTICLE

Engineering Reports
Open Access

# Design of All-Dielectric Thermal Microfluidic-based Reconfigurable Metasurface

**Ahmed AlGhamdi1[1] | Jawad Yousaf[2] | Ali Yahyaoui[1,3] | Nebras Sobahi[1] | Bandar Hakim[1] | Raj Mittra[1,4] | Hatem Rmili[1,5]**

[1]Electrical and Computer Engineering Department, Faculty of Engineering, King Abdulaziz University, P.O. Box 80204, Jeddah 21589, Saudi Arabia.

[2]Department of Electrical, Computer and Biomedical Engineering, Abu Dhabi University, United Arab Emirates.

[3]University of Tunis El Manar (UTM), National Engineering School of Tunis (ENIT), Communications Systems Laboratory (SysCom), BP 37, Belvédère 1002 Tunis, Tunisia.

[4]Electrical and Computer Engineering Department, University of Central Florida, EMC Lab, Orlando, 32816 USA.

[5]K. A. CARE Energy Research and Innovation Center, King Abdulaziz University, Jeddah 21589, Saudi Arabia

**Correspondence**
*Hatem Rmili, King Abdulaziz University, P.O. Box 80204, Jeddah 21589, Saudi Arabia.
Email: hmrmili@kau.edu.sa

**Funding Information**
Deanship of Scientific Research (DSR), King Abdulaziz University, Jeddah, Saudi Arabia under grant No. (KEP-PhD-13-135-42).

## Abstract

Metasurfaces tuning is performed using different ways for wide range of applications. This study presents the design of thermally-tuned all-dielectric reconfigurable metasurface. A microfluidic channel, filled with different concentrations of tellurium – selenium (Te-Se) alloy, is added on the top of the elliptical dielectric resonator (EDR) unit cell of the considered metasurface. The electrical properties of used semiconductor alloy are varied in the range of 400°C to 700°C (steps size of 100°C). The impact of thermal tuning on the reflection and transmission characteristics of the designed metasurface is analyzed in the frequency range 20-30 GHz using COMSOL Multiphysics. Obtained results demonstrated that the realized metasurface exhibits reconfigurable behavior in terms of variations in the reflection and transmission characteristics with a change in either temperature or concentrations of selenium and tellurium. The wider bands with high reflection and low transmission frequency bands are obtained with lower concentrations of selenium and tellurium for all operating temperatures.

## KEYWORDS

All-dielectric, metasurface, reconfigurable, microfluidic, transmission coefficient, operating temperature, tellurium – selenium alloy.

## 1 | INTRODUCTION

Metasurfaces, composed of unit cells or resonators, have been widely used in numerous RF and microwave applications. The periodic arrangement of designed sub-wavelength resonators brings a change in the wave fronts of the incident electromagnetic waves [1-4]. This principle led to the development of numerous applications using metasurfaces such as metalenses [5, 6], broadband polarization converters [7-9], THz sensors [2], holograms [11, 12], beam steering [15, 16], and absorbers [7, 17, 18], to name a few. All-dielectric metasurfaces, providing additional advantages of low losses, have gained a lot of attention for the development of reconfigurable metasurfaces [2-4, 14, 19, 20]. The dynamic control of the variations in transmission and reflection properties of the meta-atom unit cells is possible in reconfigurable metasurfaces. This is possible due to conventional approaches including the

Received: Added at production | Revised: Added at production | Accepted: Added at production
DOI: xxx/xxxx

integration of active components such as diodes, integrated circuits (IC), and MEMS [7-9, 21-24]. In particular, the electrical properties of some alloys and fluid metals were varied to obtain the reconfigurable nature of the realized broadband metasurfaces [18, 25, 26].

Recent studies [1,14, 27-33] showed that the tunable nature of metasurfaces can also be obtained by manipulating the thermal properties of the used materials. The thermal tuning of a terahertz (THz) metasurface using Indium antimonide (InSb) alloy is presented in [1]. A comprehensive analysis of the thermal tuning of the realized metasurface using different semiconductor materials of group IV-VI is presented in [31]. Chen et al. employed a split ring resonsoatr to demonstrate the temperature dependence of a THz metasurface response based on $\boldsymbol{YBa_2Cu_3O_{6.05}}$ (YBCO) alloy [32]. The same alloy was used for the analysis of non-linear thermal properties of a THz metasurface [33]. The study of [14] confirmed that electrical and magnetic resonances of an all-dielectric metasurface change with the change in the temperature or ambient refractive index of employed materials. The authors in [30] suggested that the loading of an all-dielectric optical metasurface structure with metal enhances its thermal emissions for radiative cooling applications. Authors in [27] vary the temperature in the range of 80-873 K to demonstrate the frequency-shift characteristics of metasurface based on silicon and germanium semiconductors. Recently, Wang et al., [28] demonstrated the cloaking operation of a flexible copper-graphene-based thermal metasurface.

**Table 1.** Comparison of proposed work with legacy works

| Refs | Unit cell | Alloy | Substrate | Analysis mechanism | Operation Spectrum | Analyzed Temperature |
|---|---|---|---|---|---|---|
| **[1]** | Strip resonator | Indium antimonide (InSb) | Quartz | Transmission | 0 - 1.2 THz | 450 – 250 K |
| **[10]** | Split-ring resonator | $YBa_2Cu_3O_{6.05}$ (YBCO) | $LaAlO_3$ (LAO) | Transmission | 0.2 - 0.8 THz | 20-100 K |
| **[13]** | Split-ring resonator | $YBa_2Cu_3O_{7-\delta}$ (YBCO) | $LaAlO_3$ (LAO) | Transmission | 0.2 -1.4 THz | 23-90K |
| **[14]** | Nanoblocks | Silicon | Fused Silica | Refractive index | 0.16 – 0.22 THz | 0 – 100 °C |
| **[27]** | Single spreheical Mie resonator | Si/Ge | - | Transmission | 25-150 THz | 80 K – 873 K |
| **[29]** | Dielectric resonator | VO2/SiO2/VO2 | Silicon | Absorption | 21-150 THz | 20 – 90 °C |
| **[14]** | Dielectric resonator | Silver | Dopped siliicon | Absorption | 10.7-75 THz | 200 K -600K |
| **[31]** | Single semiconductor Mie resonator | Group IV and group IV–VI semiconductors | $SiO_2$ | Reflection | 21-38 THz | 80 – 873 K |
| **This work** | Elliptical dielectric resonaotr (EDR) | Tellurium – selenium (TeSe) | Roger 3210 | Transmission and Reflection | 20 - 30 GHz | 500-600 °C |

In this work, switchable transmission and reflection characteristics of an elliptical dielectric resonator (EDR) based thermal metasurface are obtained. Figure 1 shows the realized EDR-based metasurface. The EDR is made of Rogers RO3210 substrate ($\varepsilon = 10.2$ and $\tan\delta = 0.03$). A microfluidic channel is created on the top of the EDR resonator which is then filled with

Received: Added at production | Revised: Added at production | Accepted: Added at production
DOI: xxx/xxxx

liquid semiconductor alloy of $\boldsymbol{Te_{1-x} - Se_x}$. The liquid alloy is made by combining the selenium and tellurium above their melting points. The permittivity and permeability of used semiconductor liquid selenium-tellurium alloy are 10 and 27 respectively [34, 35]. The study analyses the performance of the realized metasurface under two cases: (i) changing the concentration of the materials to form 8 different semiconductor alloys of $\boldsymbol{Te_{1-x} - Se_x}$ for 0 ≤ x ≤ 0.7 for fixed temperature ; (ii) varying the operating thermal condition of each formed alloy of $\boldsymbol{Te_{1-x} - Se_x}$ for 0 ≤ x ≤ 0.7 in the range of 400 °C to 700 °C (steps size of 100 °C). The characterization for the afore mentioned 32 case studies (combination of both 'x' and temperature) is done by analyzing the two-port S-parameters of the structure in the frequency range of 20-30 GHz. The COMSOL Multiphysics software is used for the full-wave numerical analysis of each case study. The performed analysis suggests that the role of the thermal conditions and joining concentrations of combining materials is vital in the realized reconfigurable operating nature of the proposed metasurface. The simplicity of design and ease of tuning of the switchable transmission and reflection characteristics of the realized metasurface makes it a better choice as compared to legacy approaches [7-9, 18, 21-23, 25, 26]. The main contribution of the study is demonstrating that change in the semiconductor alloy in the microfluidic channel various the dynamic transmission and reflection characteristic of all-dielectric metasurface operating in microwave frequencies. To the best of our knowledge, the proposed study is first of kind that presents a comprehensive analysis of the impact of variations in the Te-Se semiconductor alloy concentrations on the reconfigurable properties of an all dielectric metasurface (based on Roger substrate) in the microwave band.

The details of metasurface design, numerical analysis setup, case studies conditions, and discussion about the obtained results are given in the following sections.

## 2 | ALL DIELECTRIC ELLIPTICAL METASURFACE DESIGN

An all-dielectric elliptical metasurface is designed in which unit call has the shape of the elliptical dielectric resonator (EDR). Figure 1 depicts the schematic of the realized metasurface. The EDR unit cell constitutes Rogers RO3210 having a relative permittivity of 10.2 and loss tangent of 0.003. The optimized structure of EDR has a thickness (g) of 2.56 mm, minor axis radius (a) of 2.5 mm, and major axis radius (b) of 2a mm.

On the top of elliptical EDR wings, a microfluidic channel of 100 x 100 µm is created which is covered by polydimethylsiloxane (PDMS). The width of this created microfluidic channel is 0.5 mm and it has a thickness (d) of 1.1 mm. Figure 1(b) illustrates the dimensions and port definitions of the dielectric resonator unit cell. The dimensions of the EDR are $Lx$ = 9.9 mm ($Lx < \lambda$), $Ly$ = 9.9 mm ($Ly < \lambda$), and $Lz = 16\lambda$. The $\lambda$ value is calculated at the highest analyzed frequency of 30 GHz. For the periodic infinite arrangement of EDR resonators, each cell is connected with the next one through a length of ($Lx$-2a/2) and a width of 2.56 mm (g).

The installed microfluidic channel in the EDR resonator is filled with semiconductor liquid selenium-tellurium alloy of $\boldsymbol{Te_{1-x} - Se_x}$ and the temperature of the alloy was changed to analyze the impact of the temperature variations on the transmission and reflection parameters of the realized metasurface. The analysis was performed using COMOSOL 5.4 Multiphysics software in the frequency range of 20-30 GHz.

The periodic port is used as port definition and the excitation of the structure is performed through normal plane wave excitation in the z-direction. The periodic port is used because the realized metasurface is itself a periodic structure that constitutes of array of unit cells.

Received: Added at production | Revised: Added at production | Accepted: Added at production
DOI: xxx/xxxx

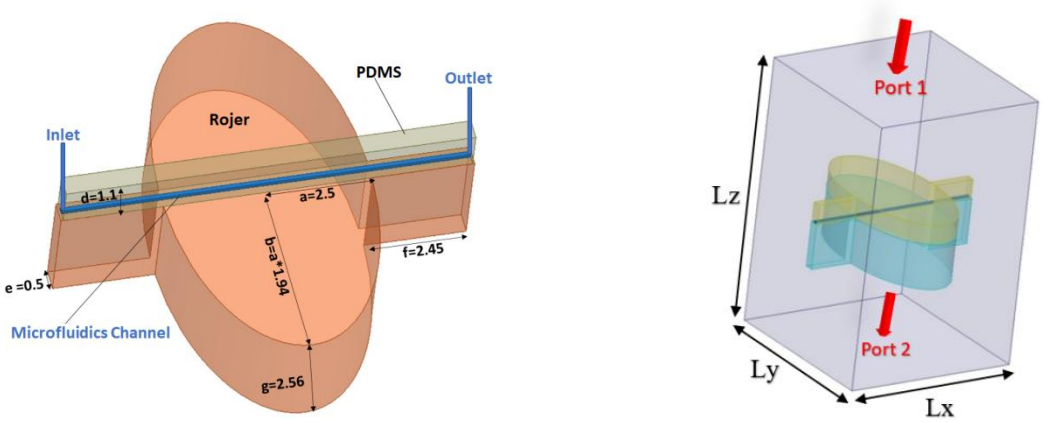


(a) (b)

**Fig. 1.** Schematic of the proposed metasurface: (a) Model configuration (all units in mm), (b) COMSOL model for the unit cell (port 1 and 2 are periodic port).

The two-port S-parameters are recorded for the entire analysis frequency band to observe the variations in the transmission and reflection properties of the realized metasurface under different thermal conditions.

## 3 | NUMERICAL ANALYSIS

The use liquid semiconductor alloy used in this study is liquid selenium-tellurium $\boldsymbol{Te_{1-x} - Se_x}$ [36]. The electrical properties (conductivity) of liquid semiconductors vary with the change in thermal conditions [36, 37]. Perron [36] did an extensive analysis of the variations in the electrical conductivity of different concentrations of selenium-tellurium liquid alloys. Based on the performed analysis of [36], different case studies are devised to analyze the thermal reconfigurability of the proposed EDR-based all-dielectric metasurface. Table 2 lists the analyzed case studies as per the presented results in [36]. The melting points of tellurium and selenium are 450 °C and 220 °C respectively [36]. The chosen case study temperature are based on their melting points to ensure that proper alloy is made when both tellurium and selenium are combined with different concentrations (i.e. x).

The change of 'x' in the liquid alloy of $\boldsymbol{Te_{1-x} - Se_x}$ produces different variants of semiconductor alloy with the change in concentrations of combined liquid materials. Each variant e.g. x = 0.05 produce liquid alloy of $\boldsymbol{Te_{1-0.05} - Se_{0.05}}$ that have different electrical conductivity based on the thermal conditions. Table 2 summarizes the changes in the electrical conductivity of the numerous versions of $\boldsymbol{Te_{1-x} - Se_x}$ under different thermal conditions. Table 2 is derived from the presented Figure 1 results in [36].

We can observe that electrical conductivity (σ) of $\boldsymbol{Te_{1-0} - Se_0}$, $\boldsymbol{Te_{1-0.05} - Se_{0.05}}$, $\boldsymbol{Te_{1-0.1} - Se_{0.1}}$, $\boldsymbol{Te_{1-0.2} - Se_{0.2}}$, $\boldsymbol{Te_{1-0.3} - Se_{0.3}}$, $\boldsymbol{Te_{1-0.4} - Se_{0.4}}$, $\boldsymbol{Te_{1-0.5} - Se_{0.5}}$, and $\boldsymbol{Te_{1-0.7} - Se_{0.7}}$ are 1.2 x 105 s/m, 7.5 x 104 s/m, 35000 s/m, 5000 s/m, 9000 s/m, 1500 s/m, 200 s/m, and 1 s/m for the 400 °C. Similar observations can be made from Table for other variants of $\boldsymbol{Te_{1-x} - Se_x}$ for different temperatures.

The conductivity of the filled $\boldsymbol{Te_{1-x} - Se_x}$ alloy in the microfluidic channel of Figure 1 EDR resonator is varied for all the mentioned cases in Table 2. For each case, two-port S-parameter results are recorded to analyze the variations in the EDR-metasurface properties which are discussed in the next section.

Received: Added at production | Revised: Added at production | Accepted: Added at production
DOI: xxx/xxxx

and |S21| ≤ -10dB. On the contrary, the frequency bands where |S11| ≤ -10dB and |S21| ≥ -5dB are referred to as high transmission and low reflection or mode 2 in this study. These modes are defined for the brevity of analysis in this study.

**Table 2.** Analyzed case studies for the different variants of $Te_{1-x} - Se_x$ under different thermal conditions

| x | Temp. °C | | | |
|---|---|---|---|---|
| | 400 | 500 | 600 | 700 |
| **0** | 1.20E+05 | 2.10E+05 | 2.60E+05 | 2.80E+05 |
| **0.05** | 7.50E+05 | 1.90E+05 | 2.40E+05 | 2.80E+05 |
| **0.1** | 35000 | 150000 | 20000 | 240000 |
| **0.2** | 5000 | 70000 | 150000 | 190000 |
| **0.3** | 9000 | 1500 | 80000 | 150000 |
| **0.4** | 1500 | 1900 | 20000 | 60000 |
| **0.5** | 200 | 300 | 4000 | |
| **0.7** | 1 | 10 | 200 | 750 |

**Table 3.** Analyses mode behaviours

| Mode | Behaviour | Conditions |
|---|---|---|
| **Mode 1** | High reflection and low transmission | \|S11\| ≥ -5dB and \|S21\| ≤ -10dB |
| **Mode 2** | High transmission and low reflection | \|S11\| ≤ -10dB and \|S21\| ≥ -5dB |

It can be noted from the Figure 2 waveforms that the designed metasurface is operating in Mode 2 i.e. high transmission and low reflection from 20 GHz – 21.5 GHz. The operational behavior of the realized structure changes to low transmission and high reflections from 21.5 GHz till around 23 GHz as for this region |S21| ≤ -10dB. The next bands where the Mode 1 operation can be noted are 26.2- 27.7 GHz, and 28.3 -29.5 GHz respectively. These results depict that the metasurface is continuously shifting among the low and high transmission regions in the analyzed frequency range of 20 to 30 GHz.

## 4 | NUMERICAL RESULTS

### 4.1 | *WITHOUT MICROFLUIDICS IN CHANNEL*

All graphics should be centered. Please ensure that any point you wish to make is resolvable in a printed copy of the paper. Resize fonts in figures to match the font in the body text, and choose line widths which render effectively in print

Firstly, the performance of the designed elliptical metasurface is analyzed without any fluid in the microfluidic channel. The transmission and reflection characteristics of Figure 2 waveforms can be divided into two main modes as illustrated in Table 4. Mode 1 presents the high reflection and low transmission behavior corresponding to the region where |S11| ≥ -5dB

Received: Added at production | Revised: Added at production | Accepted: Added at production
DOI: xxx/xxxx

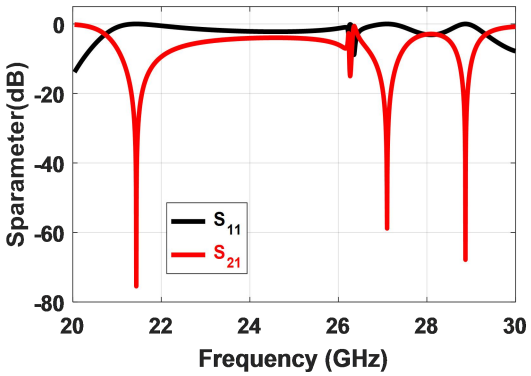


**Fig. 2.** *S*-parameters results of the model without fluids in the channel

**Table 4.** Analyses mode behaviours

| Mode | Behaviour | Conditions |
|---|---|---|
| **Mode 1** | High reflection and low transmission | \|S11\| ≥ -5dB and \|S21\| ≤ -10dB |
| **Mode 2** | High transmission and low reflection | \|S11\| ≤ -10dB and \|S21\| ≥ -5dB |

and |S21| ≤ -10dB. On the contrary, the frequency bands where |S11| ≤ -10dB and |S21| ≥ -5dB are referred to as high transmission and low reflection or mode 2 in this study. These modes are defined for the brevity of analysis in this study.

It can be noted from the Figure 2 waveforms that the designed metasurface is operating in Mode 2 i.e. high transmission and low reflection from 20 GHz – 21.5 GHz. The operational behavior of the realized structure changes to low transmission and high reflections from 21.5 GHz till around 23 GHz as for this region |S21| ≤ -10dB. The next bands where the Mode 1 operation can be noted are 26.2- 27.7 GHz, and 28.3 -29.5 GHz respectively. These results depict that the metasurface is continuously shifting among the low and high transmission regions in the analyzed frequency range of 20 to 30 GHz.

## *4.2 | WITH $Te_{1-x} - Se_x$ MICRO-FLUID IN CHANNEL*

This section details the results of the different case studies of Table 2 when the channel is filled with different variations of semiconductor alloy $\boldsymbol{Te_{1-x} - Se_x}$ for the change in x and thermal temperature. The analysis is performed for 8 different concentrations of 'x' and is detailed below.

### 4.2.1 | $Te_{1-0} - Se_0$ WITH DIFFERENT OPERATING TEMPERATURES

Figure 3 shows the reflection (S11) and transmission (S21) coefficient results of the metasurface with a microfluidic channel when we inject the channel with alloy $\boldsymbol{Te_{1-x} - Se_x}$ at x = 0 & Temp. = 400 °C. To simulate the case of $\boldsymbol{Te_{1-0} - Se_0}$ at 400 °C the alloy was assigned an electrical conductivity (σ) of 1.20E5 s/m, and the two-port S-parameters are recorded. It can be noticed by comparing Figures 2 and 3 waveforms that the insertion of the liquid alloy changes the tuning characteristics of the realized metasurface.

Received: Added at production | Revised: Added at production | Accepted: Added at production
DOI: xxx/xxxx

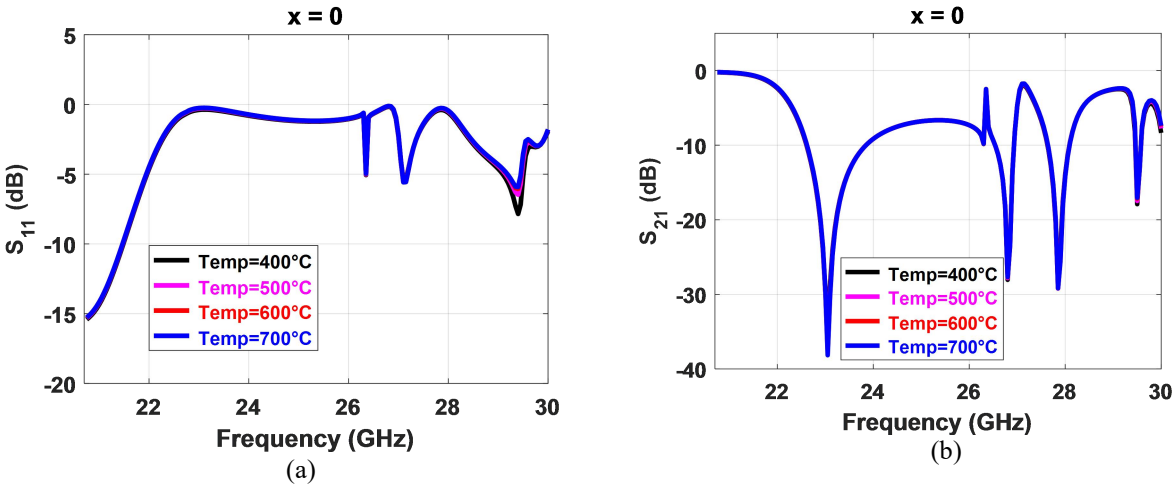


**Fig. 3.** *S*-parameters of the model with filling alloy ($Te_{1-x} - Se_x$) at $x = 0$ for different temperatures

The waveforms of Figure 3 for 400 °C shows mode 2 from 20 -21.501 GHz which makes the mode 2 operating bandwidth of around 1500 MHz It switches to mode 1 for the frequency bands of 22.6554 - 23.8578 GHz, 26.5632 - 26.964 GHz, 27.6654 - 28.1163 GHz, and 29.5191 - 29.6193 GHz. The corresponding operating bandwidths of the aforementioned mode 1's are 1202.4 MHz, 400.8 MHz, 450.9 MHz, and 100.2 MHz respectively.

The change in the temperature of $Te_{1-0} - Se_0$ to 500 °C will bring a change in its conductivity because of the change in dynamic concentrations of the minority and majority charge carriers in the semiconductor alloy. The mode 2 operation for this configuration (500 °C) is almost the same (20 -21.501) as in results of the 400 °C temperature case. For this case frequency bands of 22.6554 - 23.8578 GHz, 26.5632 - 26.964 GHz, 27.6654 - 28.1163 GHz, and 29.5191 - 29.6193 GHz represents the mode 1 operation corresponding to high reflection and low transmission region. These observe frequency bands of 500 °C waveforms are similar to like the results for 400 °C.

The observed waveforms of liquid alloy $Te_{1-0} - Se_0$ for the thermal conditions of 600 °C and 700 °C are almost the same as shown in Figure 3. This is because of no significant variations in the conductivity of the material (for all cases it's in the range of (x 105) with the change in operating temperature. This shows that the operating nature of the realized dielectric metasurface is quite insensitive to the change in operating temperature when the alloy is made by combining $Te_{1-0}$ and $Se_0$.

### 4.2.2 $|Te_{1-0.05} - Se_{0.05}$ WITH DIFFERENT OPERATING TEMPERATURES.

The second analyzed case for the inserted alloy is the mixture of liquid selenium-tellurium for x = 0.05 to form $Te_{1-0.05} - Se_{0.05}$. As like $Te_{1-0} - Se_0$, for this case analysis of the realized metasurface is performed for four different operating temperatures of 400 °C, 500 °C, 600 °C, and 700 °C respectively.

The comparison of reflection and transmission parameters result of are shown in Figure 4. The electric conductivity of the inserted liquid alloy is set to 7.05E5 to meet the analyzed operating condition for 400 °C. As the electric conductivity of the material is similar to the electric conductivity of alloy for x =0, the waveforms of Figure 4 at 400 °C look similar to Figure 3 results at 400 °C.

Received: Added at production | Revised: Added at production | Accepted: Added at production
DOI: xxx/xxxx

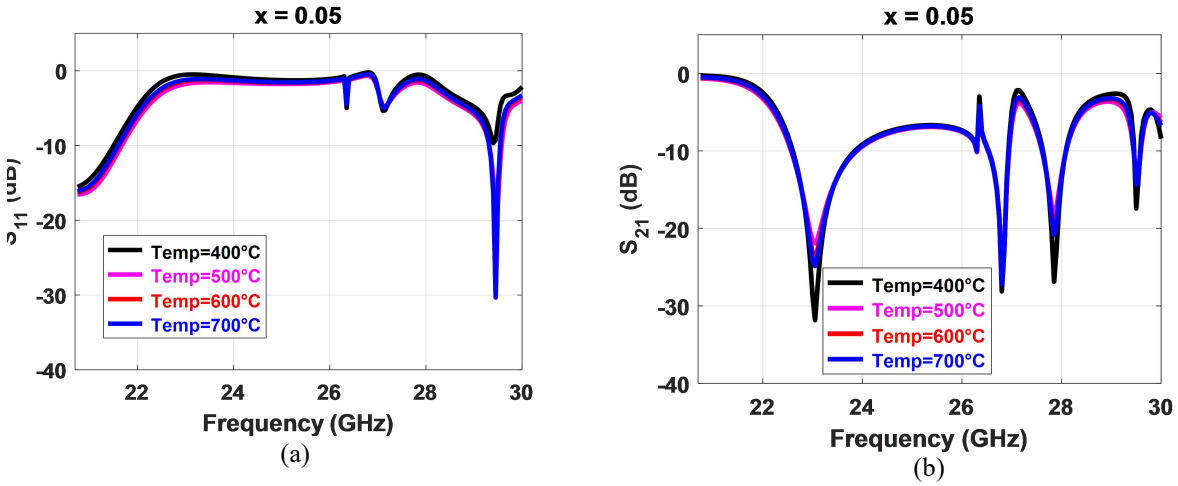


**Fig. 4.** S-parameters of the model with filling alloy ($Te_{1-x} - Se_x$) at x = 0.05 for different temperatures

At 400 °C, the high transmission and low reflection characteristic are noted in the frequency band of 20 –20.15532 GHz which are similar to the mode 2 bands of $\boldsymbol{Te_{1-0} - Se_0}$ alloy with a slight increase in the bandwidth of mode 2 from 1503 MHz to 1553.1 MHz in this case.

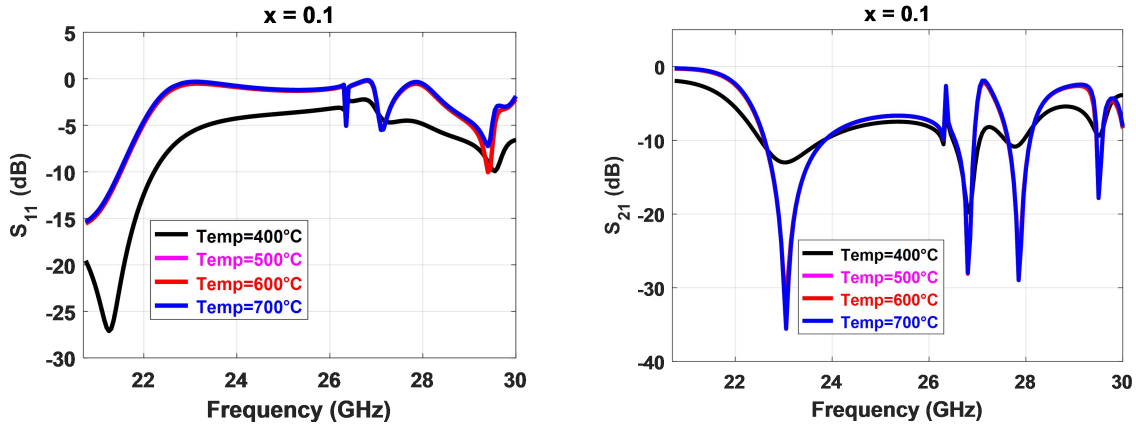


**Fig. 5.** S-parameters of the model with filling alloy ($Te_{1-x} - Se_x$) at x = 0.1 for different temperatures

The mode 1 conditions corresponding to high reflection and low transmission are observed from 22.6554 - 23.8578 GHz, 26.5632 - 26.964 GHz, and 27.6654 - 28.1163 GHz respectively. These three bands of Figure 4 waveform at 400 °C are similar to the first three bands corresponding temperature results of Figure 3.

The waveforms of S11 and S21 curves when the operating temperature of the $Te_{1-0.05} - Se_{0.05}$ is changed to 500 °C are shown in Figure 4 (pink colour waveforms). Although the waveform pattern looks similar as to earlier ones, for this case, mode 2 is noted from 20 - 21.7035 GHz which has a bandwidth of 17030 MHz here which is around 150 MHz higher than earlier cases of $Te_{1-0} - Se_0$. Then it switches to mode 1 for the bands of 22.6053 - 23.9079 GHz, 26.5632 - 26.964 GHz, and 27.6654 - 28.1163 GHz respectively. We could notice that a relatively wider band mode 1 and mode 2 operations are observed when the $Te_{1-0.05} - Se_{0.05}$ alloy is operating at 500 °C.

The change of the temperature to 600 °C and 700 °C for this alloy increase their conductivities to 2.40E05 and 2.80E05 respectively. This wider the mode 2 operating bands

Received: Added at production | Revised: Added at production | Accepted: Added at production
DOI: xxx/xxxx

to 1653.3 MHz (20 – 21.6534 MHz) for both cases (see waveforms in Figure 4) when compared to the same cases of semiconductor alloy of $\boldsymbol{Te_{1-0} - Se_0}$. Also, an increase of 100 MHz is observed for the mode 1 first operating band (22.6053-23.9079) as compared to the first operating band (22.654-23.8578) of $\boldsymbol{Te_{1-0} - Se_0}$ cases for the same operating temperatures.

The comparison reflects that combing $\boldsymbol{Te_{1-x}}$ and $\boldsymbol{Se_x}$ for x = 0.05 brings a change in the composition of the semiconductor alloy which eventually affects their electrical properties. Because of this, the operating bandwidth of the different mode 1 and mode 2 bands is enhanced for this case when compared with the same operating conditions of $\boldsymbol{Te_{1-x}}$ and $\boldsymbol{Se_x}$ for x = 0.

### 4.2.3 $|\boldsymbol{Te_{1-0.1} - Se_{0.1}}$ WITH DIFFERENT OPERATING TEMPERATURES

The change in the material compositions in the formation of $Te_{1-x} - Se_x$ for x = 0.1 decreases the overall conductivity of the alloy as compared to the earlier two cases as can be noticed from Table 2.

This will modify the transmission and reflection characteristics which can be noted from Figure 5 results for the first case i.e. $Te_{1-0.1} - Se_{0.1}$ at temp.= 400 °C. It shows mode 2 from 20.0001 - 22.2546 GHz and then it switches to mode 1 from 22.5552 - 38.857**8**, 26.5131 - 27.0642, and 27.6654 - 27.966 GHz respectively. The mode 2 operating band has a bandwidth of 2254.**6** MHz which is much higher than earlier cases. Also, mode 1 operating regions bandwidths are higher than for both earlier cases of $Te_{1-0} - Se_0$, and $Te_{1-0.05} - Se_{0.05}$ at temp.= 400 °C. This reflects the change in tuneable characteristics of the metasurface with the change in components concentrations for the fixed operating temperature.

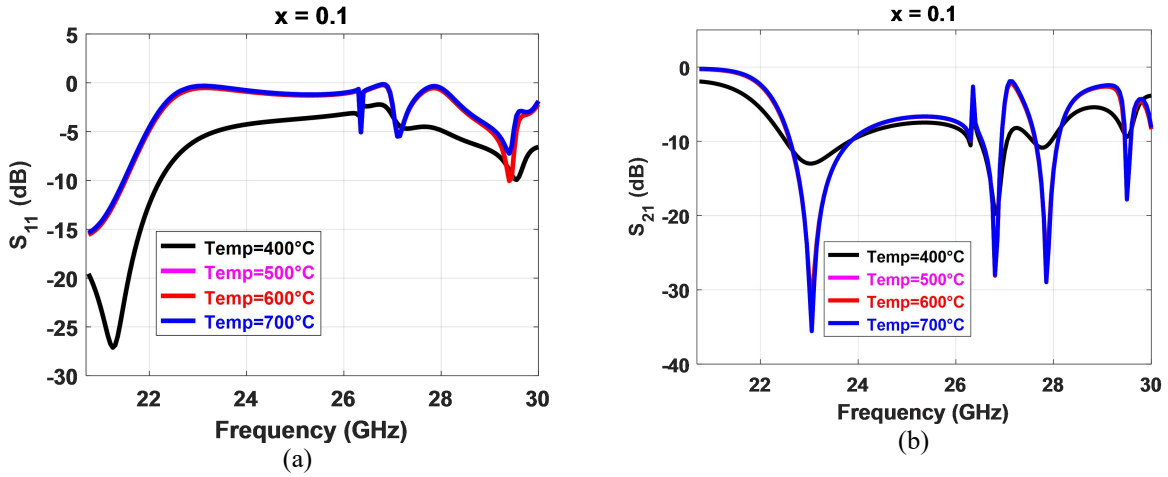


**Fig. 5.** *S*-parameters of the model with filling alloy ($Te_{1-x} - Se_x$) at $x = 0.1$ for different temperatures

The further increase in the operating temperature to 500 °C for this alloy configuration varies the transmission and reflection parameters and tune mode 1 and mode 2 to different bands as shown in Figure 5. These results are similar to Figure 3 i.e. for $Te_{1-0} - Se_0$ at 500 °C. This shows that changing of temperature to 500 °C for $Te_{1-0.1} - Se_{0.1}$ with σ = 1.5E5 s/m shows the similar behavior as of $Te_{1-0} - Se_0$ with σ = 2.10E+05, thus showing the reconfigurable nature of the proposed structure.

Received: Added at production | Revised: Added at production | Accepted: Added at production
DOI: xxx/xxxx

Although these two cases have different electrical conductivities for the same temperature, the change in the material concentrations in the semiconductor alloy produces similar results for these two cases. The same trend of similar operating bands of both modes (1 and 2) is noticed for this case and $Te_{1-0} - Se_0$ when the operating temperature is changed to 600 °C and 700 °C respectively as depicted in Figure 5. This affirms the reconfigurable nature of the proposed structure with the change in temperature and material concentrations.

### 4.2.4 $|Te_{1-0.2} - Se_{0.2}$ WITH DIFFERENT OPERATING TEMPERATURES

Figure 6 compares the reflection (S11) and transmission (S21) coefficient results of the metasurface with a microfluidic channel when we inject the channel with alloy $Te_{1-0.2} - Se_{0.2}$ and varies its operating temperate from 400 °C to 700 °C.
The electrical conductivity of metasurface is set to 5E3 s/m for the characterization of performance at 400 °C. It can be observed from Figure 6 that transmission and reflection curves for this case are different from earlier cases.

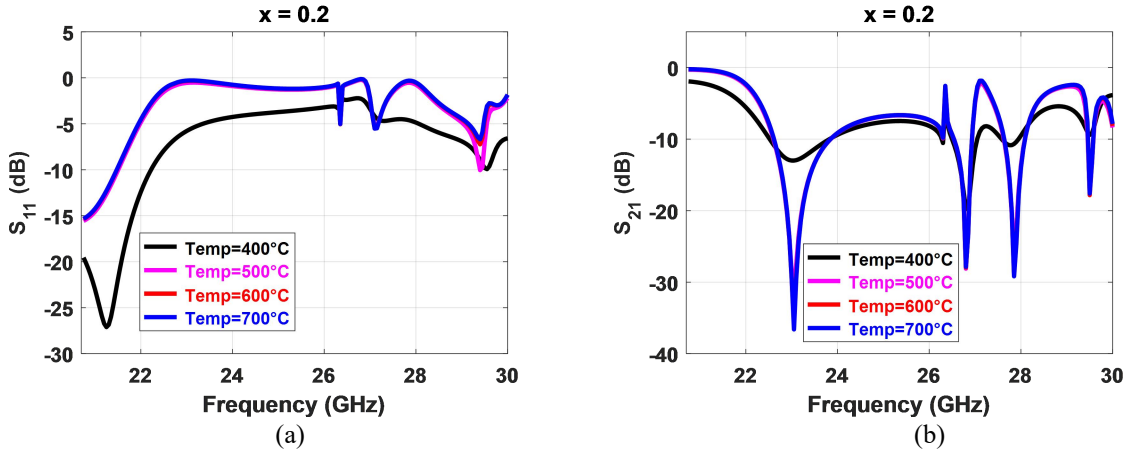


**Fig. 6.** S-parameters of the model with filling alloy ($Te_{1-x} - Se_x$) at x = 0.2 for different temperatures

At 400 °C, the observed mode 1 band for Figure 6 black curves are 22.5552 - 23.8578 GHz (1302.6 MHz), 26.5632 - 27.1143 MHz (551.1 MHz), and 27.6153 - 28.0161 GHz (414 MHz). The observed mode 2 operating band is from 20.0001 - 22.2045 GHz (2254.5 MHz). When compared with the operating modes of earlier case studies, we notice that mode 2 of this configuration $Te_{1-x} - Se_x$ at x = 0.2 & Temp. = 400 °C behaves similar to $Te_{1-x} - Se_x$ at x = 0.1 & Temp. = 400 °C with a minor change in one the mode 1 operating band. A minor difference in terms of operating bandwidths of both modes 1 and mode 2 is observed when this configurations result is compared with $Te_{1-0.1} - Se_{0.1}$ for the same temperature.
The analysis of results for the operating temperature of 600 °C reflects that mode 2 band of 20-21.5031 GHz is the same as like $Te_{1-0} - Se_0$ for the same temperature condition. The observed modes 1 band for 600 °C are 22.6554 - 23.8578 GHz, 26.5632 - 26.964 GHz, 27.6654 - 28.1163 GHz, and 29.5191 - 29.6193 GHz respectively. For the same operating temperature, these operating bands are different as compared to results obtained for $Te_{1-0.1} - Se_{0.1}$. The further increase in the temperature to 700 °C for this configuration did not bring any significant changes in the working characteristics of the same analyzed alloy case as compared to the 600 °C case.

Received: Added at production | Revised: Added at production | Accepted: Added at production
DOI: xxx/xxxx

### 4.2.5 $|Te_{1-0.3} - Se_{0.3}$ WITH DIFFERENT OPERATING TEMPERATURES

Figures 7 present the reflection and transmission curves for the semiconductor alloy of $Te_{1-0.3} - Se_{0.3}$ for the operating temperature of 400 0C, 500 °C, 600 0C, and 700 °C respectively. The conductivity of the alloy for 400 0C is 9E3 s/m which changes to 1.5E2 s/m with the change in temperature to 5000C. The other cases used conductivity can be noticed from Table 2. We could notice that the conductivities of the alloy have decreased for x = 0.3. The high transmission and low reflection characteristics are observed in the frequency domain of 20 – 21.9039 GHz. Whereas the regions corresponding to high reflection and low transmission are 22.5552 - 23.598 GHz, 26.5131 - 27.0141 GHz, and 27.6153 - 28.1163 GHz respectively.

It is noted from the curves of 600 °C that the obtained S11 and S21 changes significantly with the change in operating temperature. For this case, only mode 2 characteristic are observed from 20 to 20.952 GHz. The reconfigurable nature of the realized metasurface is observed with the further increase in temperature to 700 0C. These cases studies produce the operating bands that are similar to the obtained bands of semiconductor alloys $Te_{1-0.05} - Se_{0.05}$ (for mode 1) and $Te_{1-0.1} - Se_{0.1}$ (for mode 2) respectively.

### 4.2.6 $|Te_{1-0.4} - Se_{0.4}$ WITH DIFFERENT OPERATING TEMPERATURES

The next analyzed case study is of the change in metasurface transmission and reflection characteristics for the case of x = 0.4 i.e. $Te_{1-0.4} - Se_{0.4}$. Figure 8 depicts the S-parameter results for this case. At Temp. = 400 °C, we observed that the metasurface is only operating in mode 2 in the frequency band of 20 – 20.952 GHz. As the conductivity of the alloy for this case is the same as for the alloy concentrations with x = 0.3 at 500 °C, good similarities between this case waveforms for this can be noted by comparing the Figures 7 and 8 respectively.

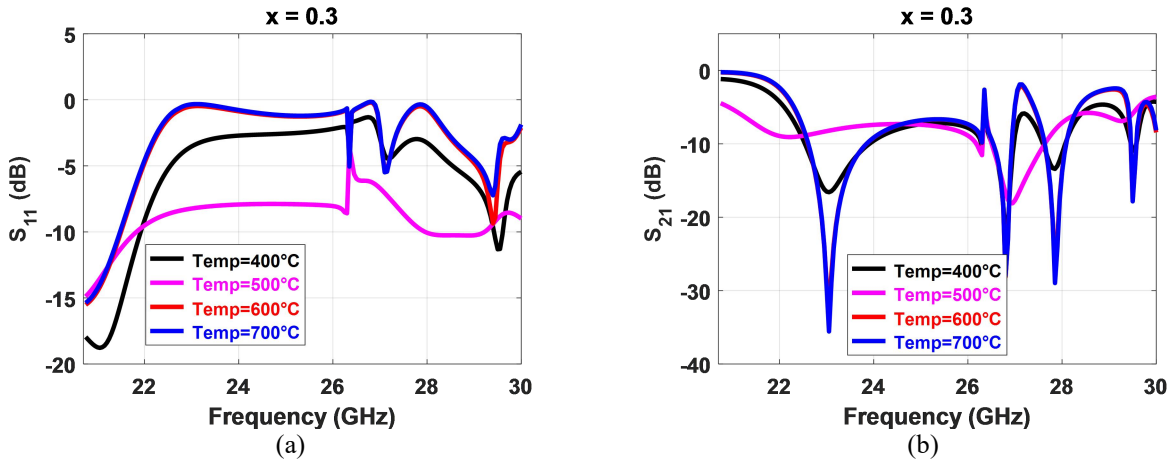


(a) (b)

**Fig. 7.** S-parameters of the model with filling alloy ($Te_{1-x} - Se_x$) at x = 0.3 for different temperatures

Received: Added at production | Revised: Added at production | Accepted: Added at production
DOI: xxx/xxxx

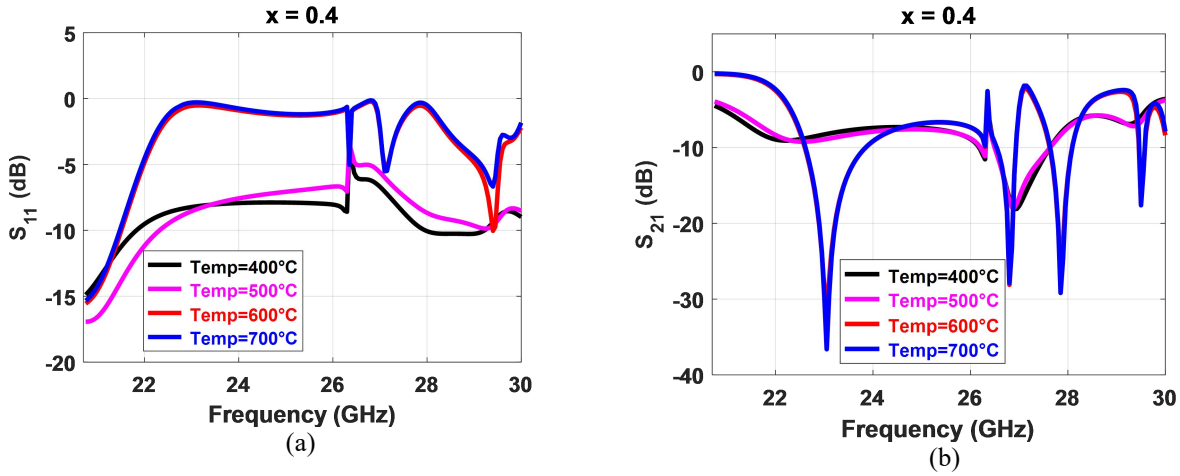


**Fig. 8.** S-parameters of the model with filling alloy ($Te_{1-x} - Se_x$) at x = 0.4 for different temperatures

The change of conductivity to 1.9E3 for the operating temperature of 500 °C did not produce a major change in the reflection and transmission parameters of the metasurface as compared in Figure 7. However, the further increase of the temperature to 600 °C produces different results of S11 and S21 as compared to the earlier two cases due to the increase in the conductivity to 2.0E4 s/m.

The bands covering mode 1 for 600 °C configuration are 26.5632 - 26.964 GHz (400.8 MHz), 27.6153 - 28.1163 GHz (450.9 MHz), and 29.5191 - 29.6193 GHz (100.2) respectively. The mode 2 operation is noted from 20 to 21.5532 GHz. It can be observed that for the same operating conditions, the earlier case of alloy for x < = 0.3 produces wider frequency bands for mode 1 and 2 operations.

### 4.2.7 $|Te_{1-0.5} - Se_{0.5}$ WITH DIFFERENT OPERATING TEMPERATURES

Figure 9 presents the variations in the reflection and transmission parameters of the metasurface when the liquid alloy is changed to $Te_{1-0.5} - Se_{0.5}$ for different analyzed operating temperatures.

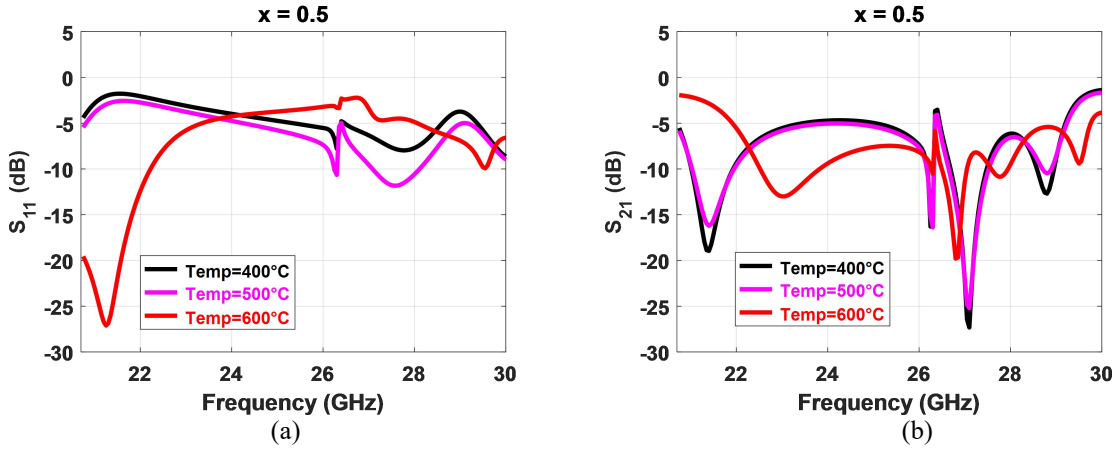


**Fig. 9.** S-parameters of the model with filling alloy ($Te_{1-x} - Se_x$) at x = 0.5 for different temperatures

Received: Added at production | Revised: Added at production | Accepted: Added at production
DOI: xxx/xxxx

The conductivity of the semiconductor alloy drops to 200 s/m for 400°C which brought the changes in the dynamic behaviour of this case as compared to earlier analyzed results. When the metasurface is operating at 400°C, the mode 2 operating band covers only 300 MHz ranging from 20-20.3007 GHz which is lowest for the all analyzed configurations of $Te_{1-x} - Se_x$ so far. Only two bands (21.0522 - 22.0041 GHz and 21.0522 - 22.0041 GHz) depicting the mode 1 characteristics can be noted from the S-parameter characteristic curves of 400°C case. The bandwidth of these afore mentioned modes 1 is also lower as compared to earlier cases for the same temperature and different concentrations of materials.

The operating frequencies for mode 1 are only 21.0522 to 22.0041 GHz for the same concentration alloy with an operating temperature of 500 °C. While the mode 2 bands remain unchanged with the change in temperature to 500 °C from 400 °C.

Due to the increase in the conductivity of the alloy for 600°C, the number of frequency regions corresponding to mode 1 characteristics increased as can be noted from Figure 9 results. For 600°C case, the mode 1 properties are observed for the ranges of 23.1564 - 23.9079 GHz, 26.5131 - 27.1143 GHz, and 27.5652 - 28.0161 GHz respectively. No frequency band depicting the mode 1 or mode 2 characteristics is noted for the $Te_{1-0.5} - Se_{0.5}$ with temperature = 700 °C.

### 4.2.8 $|Te_{1-0.7} - Se_{0.7}$ WITH DIFFERENT OPERATING TEMPERATURES

The conductivity of semiconductor alloy for x = 0.7 is 1 s/m at 400 °C as shown in Table 2. The microfluidic channel is filled with alloys having a conductivity of 1 s/m. The recorded S-parameter results are shown in Figure 10. It shows mode 2 from 20 – 20.2005 GHz and then switches to mode 1 for bands of 21.0522 - 21.954 GHz, 26.8137 - 27.4149 GHz, and 28.5672 - 29.0181 GHz respectively.

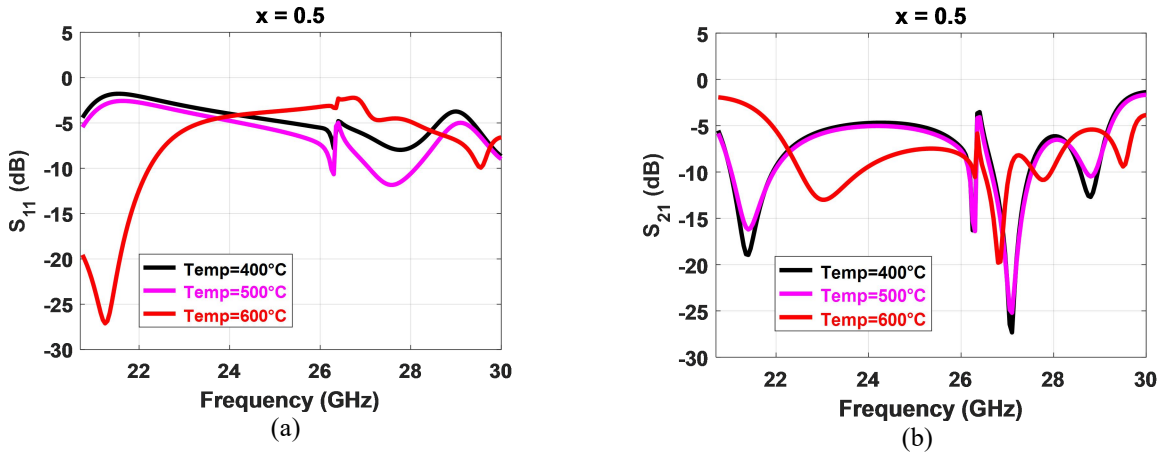


**Fig. 9.** S-parameters of the model with filling alloy ($Te_{1-x} - Se_x$) at x = 0.5 for different temperatures

The operating bandwidth of mode 2 is 200.4 MHz for this 400°C case and it remains unchanged when the operating temperature of this alloy concertation is changed to 500 °C as can be noticed in Figure 10 pink curves. The observed bandwidths for mode 1 for at 500°C are 901.8 MHz (21.0522 - 21.954 GHz), 200.4 MHz (26.1624 - 26.3628 GHz), 150.3 MHz (27.2624 - 27.4165 GHz), and 450.9 MHz (28.5672 - 29.0181 GHz).

Received: Added at production | Revised: Added at production | Accepted: Added at production
DOI: xxx/xxxx

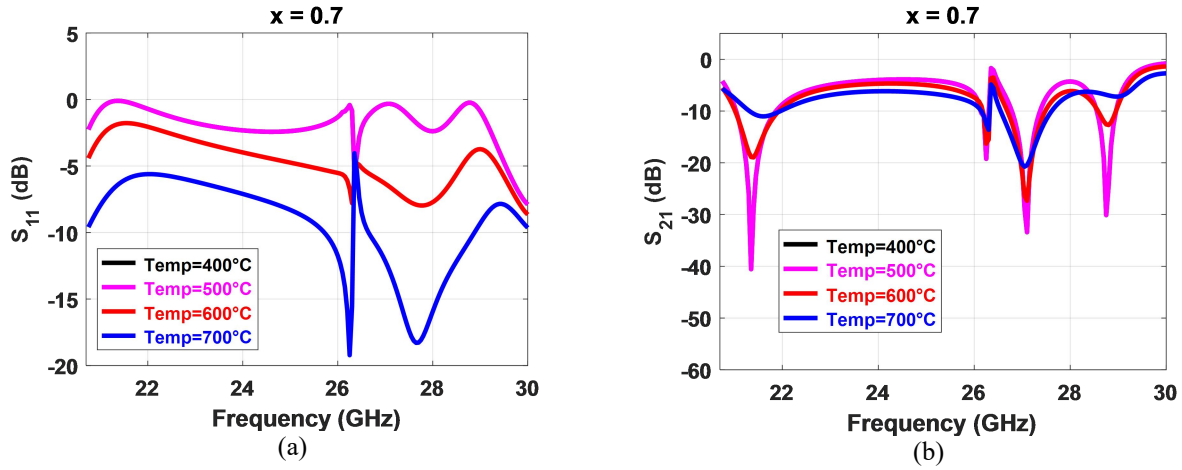


**Fig. 10.** S-parameters of the model with filling alloy ($Te_{1-x} - Se_x$) at x = 0.7 for different temperatures

The further increase of the temperature to 600°C increases the high transmission and low reflection band to 300.6 MHz (20 - 20.3007 GHz) from 200.4 MHz for earlier two cases of this alloy concentration. This increase in the operating range of mode 2 as can be noted from Figure 10 results. The variations in the bands representing the mode 1 operation can also be noticed for 600°C waveforms by comparing its curves with 400°C and 500 °C configurations respectively.

The last analyzed case study is for the operating temperature of 700 °C which changes the conductivity of the alloy to 750 s/m. The analyzed results depict that only mode 2 operation exists for this case. The observed band reflecting high transmission and low reflection region is from 20 -20.7516 GHz.

## 5 | COMPARISON AND DISUSSION

Table 4 presents a summary of high reflection and low transmission (mode 1) and high transmission and low reflection (mode 2) for all analyzed case studies of Table 2.

The comparison reflects that mode 1 is the dominant mode of operation for the realized metasurface across all case studies. The mode 1 characteristics are observed in different bands for each case study. On the contrary, the mode 2 operation has a relatively fixed band in the frequency range of 20-22.5 GHz for all analyzed cases of different concentrations of alloys.

For x = 0, the impact of temperature on both dominant operating modes is almost negligible. The same thing can be observed for other cases of x till x = 0.7. These changes of the concentrations of the joining materials (x) to form different variants of semiconductor alloy vary the operating bands of both modes. That reflects the tunable and reconfigurable nature of the proposed metasurface.

For a fixed operating temperature of 400 °C, the change in the concentrations of the semiconductor alloy $Te_{1-x} - Se_x$ from 0 to 0.2 enhances the operating bandwidth of mode 2 from 1503 MHz to 2254.5 MHz. The same trend can also be noticed for almost all operating bands corresponding to mode 1 for the fixed operating temperature of 400 °C and for $0 \leq x \leq 0.2$. The reason for this is the decrease in the conductivity of alloy from $1.5\ 10^5$ (x = 0) to $5\ 10^3$ (x = 0.2) at a temperature before the melting point of tellurium (Te). After that, although the temperature is fixed, the role of combined metals concentrations becomes

Received: Added at production | Revised: Added at production | Accepted: Added at production
DOI: xxx/xxxx

important and it results in a decrease of the operating bandwidths of both mode 1 and mode 2 for the same fixed operating temperature of 400 °C.

The overall wider frequency bands for both modes' operations are observed for the lower concentrations of both materials. The increase in the concentrations of both selenium and tellurium (e.g. for x =0.5 and x = 0.7) results in two things: (i) overall decrease in the bandwidths of both modes, (ii) decrease in the number of operating bands for mode 1. The reason for this is the reduction in the overall conductivity of the alloy for these cases as compared to the other cases. The nature of the used alloy becomes more insulators (lesser conductive) with the increase in the concentration of both selenium-tellurium. This reduces the both number of operating modes and their respective bandwidths for these cases. This shows that even for a fixed temperature, the switchable nature of the realized metasurface could be obtained by just varying the materials combinations.

Another important aspect of the realized metasurface is that nearly similar transmission and reflections characteristics can be tuned for different/same thermal conditions by varying the concentrations levels. The examples of such cases are (i) $Te_{1-0.1} - Se_{0.1}$ at temp. = 600 °C and $Te_{1-0} - Se_0$ at temp. = 500 °C; (ii) $Te_{1-0.2} - Se_{0.2}$ at temp. = 600 °C/700 °C and $Te_{1-0} - Se_0$ at temp. = 600 °C/700 °C; and (iii) $Te_{1-0.2} - Se_{0.2}$ at temp. = 600 °C and $Te_{1-0} - Se_0$ at temp. = 400 °C. The reason for such similar characteristics is the comparable conductivities of the alloy for these cases.

The comparison of Table 4 and Figures 3-10 depicts that the operating characteristics of the realized metasurface can be easily tuned for different bands of high reflection and low transmission and vice versa by playing either with the operating temperature or the joining concentrations of metals to form different version of inserted alloy in the microfluidic channel.

Analysis of the electromagnetic field distribution in figures11 and 12 revels that the magnitude of the electric field in the microfluidic channel increase with increasing the ratio x of Selenium within the alloy at the selected frequencies.

This increase is more significant for T=400°C than T= 600°C. This behaviour may be attributed to the large increase in hole mobility with atomic ration x of selenium as explained in [36] and the trend to the metallic state at high temperature [36].

We can also note from figures 11 and 12, the presence of two different configurations for both electric and magnetic fields at all the selected frequencies, which confirm the presence of two resonating modes within the structure.

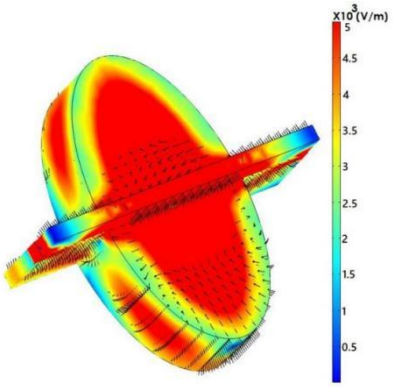


*x* = 0 @ Freq.= 23GHz

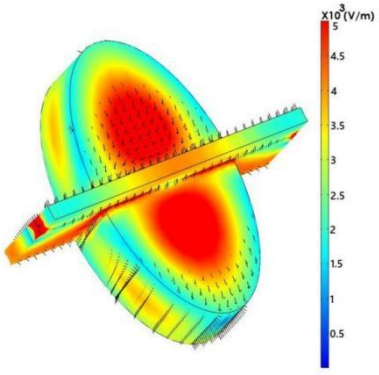


*x* = 0 @ Freq.= 20.5 GHz

Received: Added at production | Revised: Added at production | Accepted: Added at production
DOI: xxx/xxxx

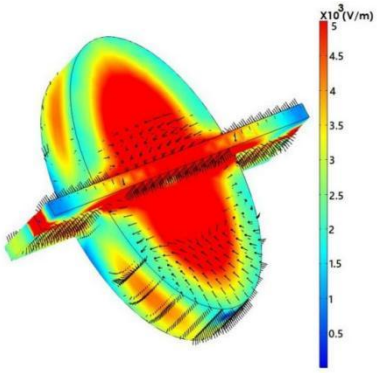


$x$ = 0.3 @ Freq.= 23GHz

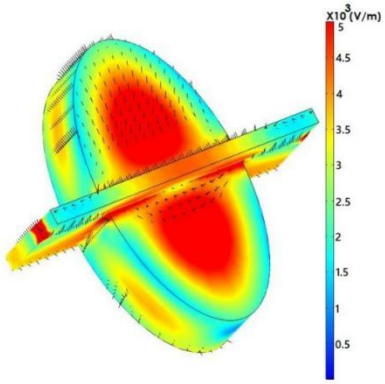


$x$ = 0.3 @ Freq.= 21 GHz

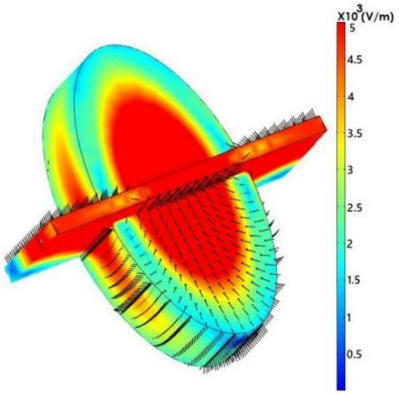


$x$ = 0.7 @ Freq.= 21.5GHz

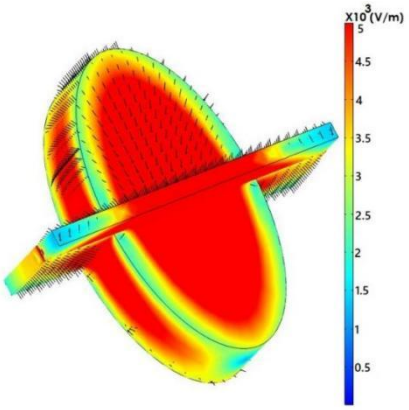


$x$ = 0.7 @ Freq.= 20.5 GHz

**Mode 1** **Mode 2**

**Fig. 11.** Mode (1) and Mode (2) Electric field norm as Multislice (V/m) and Magnetic Field as Arrow at Temp = 400 C° for different values of x

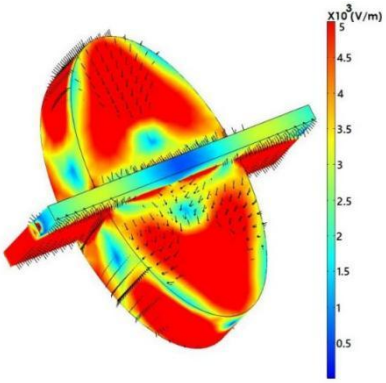


$x$ = 0 @ Freq.= 26.8 GHz

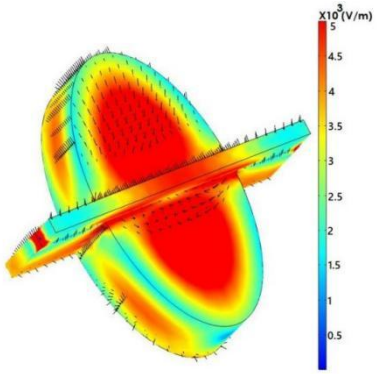


$x$ = 0 @ Freq.= 21 GHz

Received: Added at production | Revised: Added at production | Accepted: Added at production
DOI: xxx/xxxx

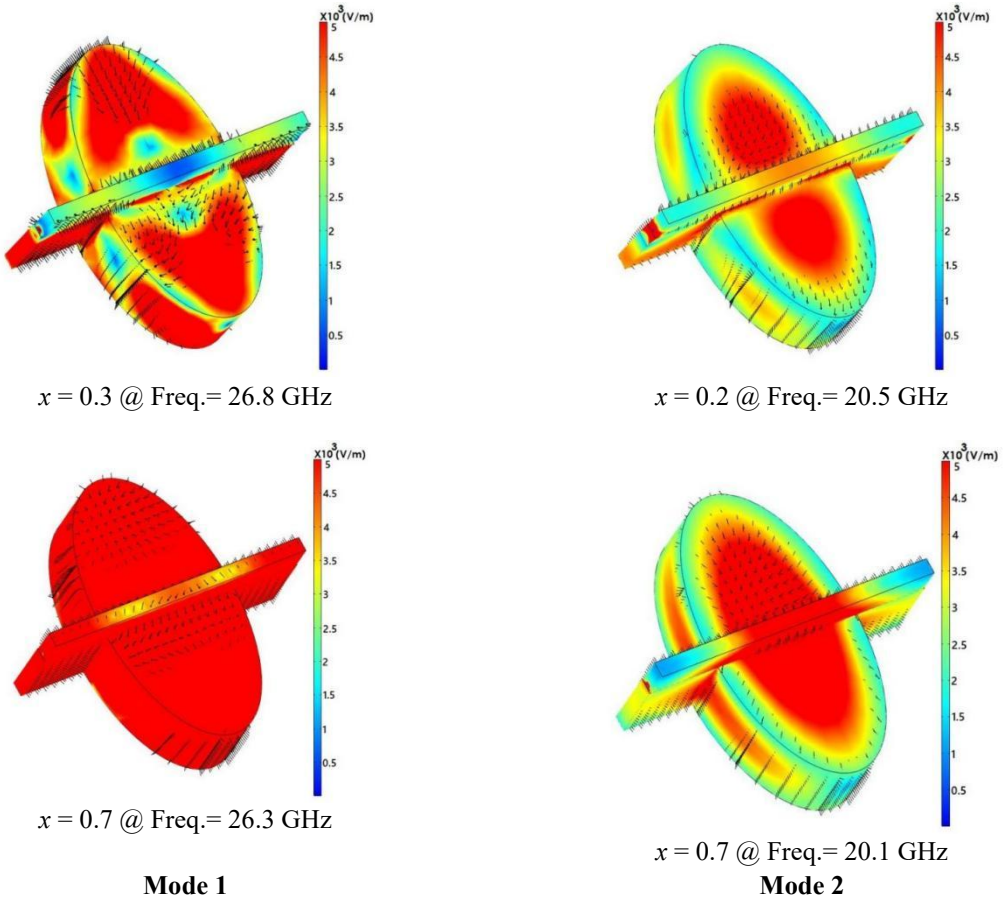


$x$ = 0.3 @ Freq.= 26.8 GHz

$x$ = 0.2 @ Freq.= 20.5 GHz

$x$ = 0.7 @ Freq.= 26.3 GHz

$x$ = 0.7 @ Freq.= 20.1 GHz

**Mode 1** **Mode 2**

**Fig. 12.** Mode (1) and Mode (2) Electric field norm as Multislice (V/m) and Magnetic Field as Arrow at Temp = 600 C° for different values of x

However, the magnetic field in the microfluidic channel tunnels seems to be not affected by the changes in Selenium ratio x or temperature, which means there no magnetic properties of the alloy in the studied frequency band 20-30 GHz.

The findings of this study could be used as a guideline for the design of thermally tuned dielectric metasurfaces. The analysis of the transmission/reflection characteristics of the realizing metasurface for different temperature conditions can be performed efficiently using the proposed technique. The obtained results using the proposed method could be beneficial for the fabrications of the designed metasurface as the optimized design parameters and concentrations of the used semiconductor alloy will reduce the cost of fabrication of different fabricated versions.

## 6 | CONCLUSION

The work has presented an extensive analysis of the impact of the operating temperature (400 °C - 700 °C with a step size of 100 °C) and concentrations of the materials to form a semiconductor alloy ( $Te_{1-x} - Se_x$ for $0 \leq x \leq 0.7$) on the transmission and reflection properties of an all-dielectric EDR-based metasurface. The performed analysis demonstrated that realized metasurface mainly operates in the high reflection and low transmission mode for the wider frequency bands as compared to low reflection and high transmission frequency ranges for all analyzed 32 case studies. The tuning of the mode's operation was noticed for

both the change in material combinational concentrations and varying thermal conditions. The switching properties are more sensitive to the change in material combinations or the fixed thermal condition i.e., operating temperature of the metasurface. The performance, although depicts reconfigurable nature, decorates in terms of mode's operating bandwidths with the increase in materials concentrations after x = 0.5. This deduces that better performance of the proposed EDR-based metasurface can be obtained with lower concentrations of both Te and Se materials in the used alloy in the microfluidic channel of the studied metasurface.

## ACKNOWLEDGEMENTS

This project was funded by the Deanship of Scientific Research (DSR), King Abdulaziz University, Jeddah, Saudi Arabia under grant No. (KEP-PhD-13-135-42). The authors, therefore, acknowledge with thanks DSR technical and financial support.

## CONFLICT OF INTEREST

The authors declared that they have no conflicts of interest to this work. We declare that we do not have any commercial or associative interest that represents a conflict of interest in connection with the work submitted.

## REFERENCES

[1]C. Luo, D. Li, J. Yao, and F. Ling, "Direct thermal tuning of the terahertz plasmonic response of semiconductor metasurface," *Journal of Electromagnetic Waves and Applications,* vol. 29, no. 18, pp. 2512-2522, 2015/12/12 2015.

[2]W. Shi *et al.*, "Terahertz Sensing for R/S Chiral Ibuprofen via All-Dielectric Metasurface with Higher-Order Resonance," *Applied Sciences,* vol. 11, no. 19, 2021.

[3]M. Y. Shalaginov *et al.*, "Reconfigurable All-dielectric Metasurfaces based on Optical Phase change Materials: Design Approaches," in *2020 International Applied Computational Electromagnetics S°Ciety Symposium (ACES)*, 2020, pp. 1-2.

[4]A. Karvounis, B. Gholipour, K. F. MacDonald, and N. I. Zheludev, "All-dielectric phase-change reconfigurable metasurface," *Applied Physics Letters,* vol. 109, no. 5, p. 051103, 2016/08/01 2016.

[5]J. Zhang, X. Wei, I. D. Rukhlenko, H.-T. Chen, and W. Zhu, "Electrically Tunable Metasurface with Independent Frequency and Amplitude Modulations," *ACS Photonics,* vol. 7, no. 1, pp. 265-271, 2020/01/15 2020.

[6]E. Arbabi, A. Arbabi, S. M. Kamali, Y. Horie, M. Faraji-Dana, and A. Faraon, "MEMS-tunable dielectric metasurface lens," *Nature Communications,* vol. 9, no. 1, p. 812, 2018/02/23 2018.

[7]J. Wang, R. Yang, R. Ma, J. Tian, and W. Zhang, "Reconfigurable Multifunctional Metasurface for Broadband Polarization Conversion and Perfect Absorption," *IEEE Access,* vol. 8, pp. 105815-105823, 2020.

[8]G. Liu, H. Liu, J. Han, Y. Mu, and L. Li, "Reconfigurable metasurface with polarization-independent manipulation for reflection and transmission wavefronts," *Journal of Physics D: Applied Physics,* vol. 53, no. 4, p. 045107, 2019/11/18 2019.

[9]Y. Li, Y. Wang, and Q. Cao, "Design of a Multifunctional Reconfigurable Metasurface for Polarization and Propagation Manipulation," *IEEE Access,* vol. 7, pp. 129183-129191, 2019.

[10] H. T. Chen *et al.*, "Tuning the resonance in high-temperature superconducting terahertz metamaterials," *Phys Rev Lett,* vol. 105, no. 24, p. 247402, Dec 10 2010.
[11] R. C. Devlin, M. Khorasaninejad, W. T. Chen, J. Oh, and F. Capasso, "Broadband high-efficiency dielectric metasurfaces for the visible spectrum," *Pr°Ceedings of the National Academy of Sciences,* vol. 113, no. 38, p. 10473, 2016.
[12] Z. Li *et al.*, "Dielectric Meta-Holograms Enabled with Dual Magnetic Resonances in Visible Light," *ACS Nano,* vol. 11, no. 9, pp. 9382-9389, 2017/09/26 2017.
[13] N. K. Grady *et al.*, "Nonlinear high-temperature superconducting terahertz metamaterials," *New Journal of Physics,* vol. 15, no. 10, 2013.
[14] C. Zou *et al.*, "Metal-Loaded Dielectric Resonator Metasurfaces for Radiative Cooling," *Advanced Optical Materials,* https://doi.org/10.1002/adom.201700460 vol. 5, no. 20, p. 1700460, 2017/10/01 2017.
[15] E. Rahamim, D. Rotshild, and A. Abramovich, "Performance Enhancement of Reconfigurable Metamaterial Reflector Antenna by Decreasing the Absorption of the Reflected Beam," *Applied Sciences,* vol. 11, no. 19, 2021.
[16] S. Tian, H. Liu, and L. Li, "Design of 1-Bit Digital Reconfigurable Reflective Metasurface for Beam-Scanning," *Applied Sciences,* vol. 7, no. 9, 2017.
[17] S. Yin *et al.*, "Reconfigurable Chiral Metasurface Absorbers Based on Liquid Crystals," *IEEE Photonics Journal,* vol. 10, no. 6, pp. 1-9, 2018.
[18] H. K. Kim, D. Lee, and S. Lim, "Wideband-Switchable Metamaterial Absorber Using Injected Liquid Metal," *Scientific Reports,* vol. 6, no. 1, p. 31823, 2016/08/22 2016.
[19] A. Yahyaoui and H. Rmili, "Chiral All-Dielectric Metasurface Based on Elliptic Resonators with Circular Dichroism Behavior," *International Journal of Antennas and Propagation,* vol. 2018, p. 6352418, 2018/04/19 2018.
[20] A. Yahyaoui, H. Rmili, M. Sheikh, A. Dobaie, L. Laadhar, and T. Aguili, "Design of all-dielectric half-wave and quarter-wave plates microwave metasurfaces based on elliptic dielectric resonators," *ACES Journal,* vol. 32, no. 3, pp. 229-236, 2017.
[21] A. Pitilakis *et al.*, "A multi-functional reconfigurable metasurface: Electromagnetic design accounting for fabrication aspects," *IEEE Transactions on Antennas and Propagation,* pp. 1-1, 2020.
[22] K. V. Mishra, J. A. Hodge, and A. I. Zaghloul, "Reconfigurable Metasurfaces for Radar and Communications Systems," in *2019 URSI Asia-Pacific Radio Science Conference (AP-RASC)*, 2019, pp. 1-4.
[23] S. Sun, W. Jiang, S. Gong, and T. Hong, "Reconfigurable Linear-to-Linear Polarization Conversion Metasurface Based on PIN Diodes," *IEEE Antennas and Wireless Propagation Letters,* vol. 17, no. 9, pp. 1722-1726, 2018.
[24] S. Zahra *et al.*, "Electromagnetic Metasurfaces and Reconfigurable Metasurfaces: A Review," (in English), Review vol. 8, no. 615, 2021-January-14 2021.
[25] K. Ling, H. K. Kim, M. Yoo, and S. Lim, "Frequency-Switchable Metamaterial Absorber Injecting Eutectic Gallium-Indium (EGaIn) Liquid Metal Alloy," *Sensors,* vol. 15, no. 11, 2015.
[26] P. C. Wu *et al.*, "Broadband Wide-Angle Multifunctional Polarization Converter via Liquid-Metal-Based Metasurface," *Advanced Optical Materials,* https://doi.org/10.1002/adom.201600938 vol. 5, no. 7, p. 1600938, 2017/04/01 2017.
[27] T. Lewi, N. A. Butakov, and J. A. Schuller, "Thermal tuning capabilities of semiconductor metasurface resonators," *Nanophotonics,* vol. 8, no. 2, pp. 331-338, 2019.
[28] J. Wang, L. Qin, and W. Xu, "Flexible and high precision thermal metasurface," *Communications Materials,* vol. 2, no. 1, p. 89, 2021/09/01 2021.
[29] S.-R. Wu, K.-L. Lai, and C.-M. Wang, "Passive temperature control based on a phase change metasurface," (in eng), *Scientific reports,* vol. 8, no. 1, pp. 7684-7684, 2018.

Received: Added at production | Revised: Added at production | Accepted: Added at production
DOI: xxx/xxxx

[30] C. Zou *et al.*, "Metal-Loaded Dielectric Resonator Metasurfaces for Radiative Cooling," *Advanced Optical Materials,* vol. 5, p. 1700460, 08/11 2017.
[31] T. Lewi *et al.*, "Thermally Reconfigurable Meta-Optics," *IEEE Photonics Journal,* vol. 11, no. 2, pp. 1-16, 2019.
[32] H.-T. Chen *et al.*, "Tuning the Resonance in High-Temperature Superconducting Terahertz Metamaterials," *Physical Review Letters,* vol. 105, no. 24, p. 247402, 12/10/ 2010.
[33] N. K. Grady *et al.*, "Nonlinear high-temperature superconducting terahertz metamaterials," *New Journal of Physics,* vol. 15, no. 10, p. 105016, 2013/10/18 2013.
[34] L. D. Geoffrion and G. Guisbiers, "Physico-chemical properties of selenium–tellurium alloys across the scales," *Nanoscale Advances,* 10.1039/D1NA00087J vol. 3, no. 14, pp. 4254-4270, 2021.
[35] R. S. Rahman, M. Shoab, Z. M. S. H. Khan, Z. Aslam, K. Asokan, and M. Zulfequar, "Bandgap tunability endowed by isovalent sulphur doping in SeTe glassy films: Correlation with Kastner's and single oscillator models," *Journal of Alloys and Compounds,* vol. 835, p. 155441, 2020/09/15/ 2020.
[36] J. C. Perron, "Electrical and thermoelectrical properties of selenium-tellurium liquid alloys," *Advances in Physics,* vol. 16, no. 64, pp. 657-666, 1967/10/01 1967.
[37] A. M. Vora, "Study of electrical transport properties of liquid semiconductor binary alloys using pseudopotential theory," *Physics and Chemistry of Liquids,* vol. 49, no. 4, pp. 493-507, 2011/07/01 2011.